Screen Anti-influenza Lead Compounds That Target the PA$_C$ Subunit of H5N1 Viral RNA Polymerase

Lin Li[1,3,9], Shenghai Chang[2,3,9], Junfeng Xiang[1], Qian Li[1,3], Huanhuan Liang[2], Yalin Tang[1]*, Yingfang Liu[2]*

1 Beijing National Laboratory for Molecular Sciences (BNLMS), Center for Molecular Sciences, State Key Laboratory for Structural Chemistry of Unstable and Stable Species, Institute of Chemistry, Chinese Academy of Sciences, Beijing, China, 2 National Laboratory of Biomacromolecules, Institute of Biophysics, Chinese Academy of Sciences, Beijing, China, 3 Graduate University, Chinese Academy of Sciences, Beijing, P. R. China

Abstract

The avian influenza (H5N1) viral RNA polymerase protein PA$_C$ was used as a target to screen nine chlorogenic acid derivatives for their polymerase inhibitor activity. Among them, seven compounds were PA$_C$ ligands, and four inhibited influenza RNA polymerase activity. These results aid in the design of anti-influenza agents based on caffeoylquinic acid.

Introduction

Influenza virus, which has high rates of morbidity and mortality, is one of the major causes of viral respiratory infections. This virus mutates frequently, spreads rapidly, and occasionally transfers from animals to humans (e.g., avian influenza A, H5N1) [1]. The increasing geographic distribution of this epizootic virus has aroused serious concerns about the therapeutic methods currently available to curb a potential pandemic of this disease. To treat influenza, two classes of anti-influenza agents, M2 ion channel blockers and neuraminidase (NA) inhibitors, have been used [2,3]. However, the emergence of drug-resistant viruses has limited the effectiveness of these drugs [4–6]. Therefore, alternative anti-influenza agents with a low risk of drug resistance are urgently needed.

In the search for a new generation of anti-influenza drugs, the RNA polymerase has been a valuable target to confront the disease [7–9]. This heterotrimer, which contains PB1, PB2 and PA subunits, is responsible for viral RNA (vRNA) replication and transcription. Structural analysis of the PA subunit revealed several potential active sites. Mutations of certain residues in these sites could significantly reduce the polymerase activity or disrupt vRNA replication [10–16]. Moreover, the structure of the PA subunit is conserved across type A, B and C influenza viruses. This conservation indicates that the anti-influenza agents targeting the PA subunit may be effective against most influenza strains and less susceptible to drug resistance [10–12]. Actually, some works have been done in the anti-influenza molecule screening targeting at PA [17–19]. In the pursuit of novel anti-influenza agents, we present a screen against the carboxyl-terminal domain of PA (termed PA$_C$, residues 257–716).

Results and Discussion

In previous work, we have discovered chlorogenic acid (CA) from *Flos Lonicera Japonica* and *Eucommia Ulmoides Oliv* extracts as a PA$_C$ ligand and potential anti-influenza active compound [17]. Herein, nine CA derivatives, the principal active components of several anti-influenza traditional Chinese medicines (e.g., *Flos Lonicera Japonica* [20], *Stemona Japonica* [21]), were tested (Table 1, Table S1). To guide in the discovery of PA$_C$ ligands, flexible docking simulations were utilized to evaluate the binding affinities between the compounds and the target. The docking was carried out using the AutoDock (v.4.01) software package with active sites established according to the structural analysis of PA$_C$ [9]. The results were shown in Table S2 and Figure S9, S10, S11, S12, S13, S14, S15, S16, and S17, and binding affinities were summarized in Table 2. The binding affinities were scaled by pK_d values, where pK_d is the negative logarithm of the dissociation constant of the binding complex. Larger pK_d values indicate stronger binding affinities. The docking results suggested that candidate compounds **a–g** are potential binders of PA$_C$.

The binding between the candidate compounds and PA$_C$ was determined experimentally by analyzing the transverse relaxation change of the small molecule upon the addition of protein in a relaxation-edited NMR (Figure 1, Figure S1, S2, S3, S4, S5, S6, S7, and S8). As shown in Figure 1, the application of the Carr-Purcell-Meiboom-Gill (CPMG) spin-lock can suppress or even eliminate the fast-relaxing signals [22,23] from the PA$_C$ ligand. By using this method, seven of the nine compounds were confirmed to be PA$_C$ ligands (candidates **a**, **b**, **c**, **d**, **e**, **f**, and **g**).

Afterward, the binding affinities of these compounds were evaluated by transverse relaxation simulation based on NMR (Figure S18, S19, S20, S21, and S22) and kinetics simulation in surface plasmon resonance (SPR) (Figure S23, S24, S25, S26, S27, S28, and S29). The results were summarized in Table 2. From this data, the disubstituted caffeoylquinic acids (**a**, **b**, **c**, **d**, **e**) exhibited higher binding affinities to PA$_C$ relative to caffeic acid alone, quinic acid alone, and monosubstituted caffeoylquinic acids (**f**, **g**).

Table 1. Candidate compounds in screening.

Candidates	Compound name
a	3,4-dicaffeoylquinic acid
b	1,5-dicaffeoylquinic acid
c	4,5-dicaffeoylquinic acid
d	3,5-dicaffeoylquinic acid
e	1,3-dicaffeoylquinic acid
f	5-caffeoylquinic acid
g	4-caffeoylquinic acid
h	quinic acid
i	caffeic acid

doi:10.1371/journal.pone.0035234.t001

Thus, the number and position of caffeoyls on quinic acid is an important factor in PA_C binding. On the other hand, although the docking simulation predicted that candidate **b** would bind tightly to the target, experimentally this compound behaved oppositely in affinity evaluation by NMR and SPR. This may be due to steric hindrance of the bulky trans-disubstitution of caffeoyl at the 1- and 3- position of the quinic acid. Other disubstitutedcaffeoyl quinic acids bind to PA_C with high affinities because the caffeoyls are either cis-disubstituted or both in equatorial positions.

In order to address specificity of the binding, the interaction between compound **a** and Human Serum Albumin (HSA) was evaluated by relaxation-edited NMR. As shown in Supporting Information (Figure S30), compound **a** did not specifically interact with HSA.

The PA_C subunit is essential in influenza's RNA polymerase activity, so one may expect that PA_C ligands should inhibit RNA polymerase activity as well. The effects of these compounds on polymerase activity were evaluated by an ApG primer extension assay [24]. The polymerase can use ApG as a primer to synthesize cRNA from vRNA promoters; therefore, the length of cRNA can be used to judge polymerase activity. As shown in Figure 2, the candidate compounds **a**, **b**, **c**, and **d** inhibited the synthesis of cRNA while candidate **f** showed slight inhibition. The inhibition rates of compound **a**, **b**, **c**, **d**, and **f** on polymerase activity were 73%, 54%, 81%, 67%, and 26%, respectively. Notably, candidate

Table 2. Binding affinities of candidate compounds toward PA_C evaluated by visual docking, NMR, and SPR.

Cadidates	Visual docking (pK_d)	NMR[a] (pK_d)	SPR (pK_d)
a	6.75	5.80	6.00
b	6.61	5.72	5.72
c	6.82	5.05	5.03
d	6.56	4.89	4.85
e	6.66	3.89	3.47
f	6.24	—	3.33
g	5.89	—	1.85
h	4.87	—	—
i	4.89	—	—

[a]Candidates **f** and **g** were identified to be PA_C ligands, but the binding affinities were too weak to be evaluated by NMR methods.
doi:10.1371/journal.pone.0035234.t002

e enhanced the polymerase activity at a rate of 42%. Although these compounds were assayed at relatively high concentrations (5 mM), the discovery of the inhibition effectiveness on polymerase activity of these CA derivatives suggests that CA could be a lead structure for potential anti-influenza drugs. These results clearly show that disubstituted caffeoylquinic acids with low steric hindrance are more likely to be effective inhibitors against polymerase because they bind strongly to PA_C. It was also observed that some PA_C ligands did not exhibit activity in the ApG assay. This may well be due to their non-specific or weak binding to PA_C.

In summary, the avian influenza viral RNA polymerase protein PA_C, a conserved key target in the design of a new generation of anti-influenza agents, was used to screen lead plant-derived anti-influenza compounds. Seven compounds were identified as PA_C ligands. Among them, four compounds inhibited polymerase activity. Therefore, PA_C made a useful target to screen for anti-influenza agents. Based on the structure-activity relationship of CA derivatives as polymerase inhibitors, the position and number, and maybe also the synergistic effect, of the caffeoyls in quinic acid played important roles in the inhibition potential of polymerase activity. These results provided an important step in caffeoylquinic acid structure-based design of anti-influenza agents.

Materials and Methods

Materials

1,5-dicaffeoylquinic acid, 1,3-dicaffeoylquinic acid, 3,5-dicaffeoylquinic acid, 3,4-dicaffeoylquinic acid, 4,5-dicaffeoylquinic acid, 5-caffeoylquinic acid, 4-caffeoylquinic acid, quinic acid, and caffeic acid were purchased from Chengdu Mansite Pharmacetical Co., Ltd. (Sichuan, China). D_2O and 3-(trimethylsilyl) propionic acid-d_4 (TSP-d_4) sodium salt were purchased from Sigma Co. (USA).

Protein expression and purification

Methods for the preparation of PA_C protein were previously described [9]. Briefly, residues 257–716 of the PA subunit of avian H5N1 influenza A virus (A/goose/Guangdong/1/96) were cloned into a pGEX-6p vector (GE Healthcare) and transformed into *Escherichia coli* strain BL21. Cells were cultured in LB medium at 37°C with 100 mg/L of Ampicillin. When the OD600 reached 0.6–0.8, the culture was induced with 0.5 mM isopropyl-thio-D-glactosidase (IPTG) at 16°C. After 20 hours of incubation, the cells expressing PA_C were harvested and combined by centrifugation at 5000 rpm for 10 min. Recombinant protein was purified with a glutathione affinity column (GE Healthcare). Glutathione S-transferase (GST) was cleaved with PreScission protease (GE Healthcare), and the protein complex was further purified by Q sepharose FF ion exchange chromatography and Superdex-200 gel filtration chromatography (GE Healthcare). Methods for the preparation of the RNA polymerase were previously described [25]. Briefly, the RNA polymerase (PA, PB1, and PB2) complex was expressed in hi5 insect cell and purified by Ni-affinity column, ion-exchange column, and gel exclusion chromatography.

The affinity analysis based on virtual docking

To predict the binding affinities between candidate compounds and PA_C, the simulated flexible docking of ligands was carried out using the AutoDock (v.4.01) software package. The structure of PA_C was retrieved from the Protein Data Bank (PDB entries: 3CM8) and modified for visual docking. First, in the PDB file,
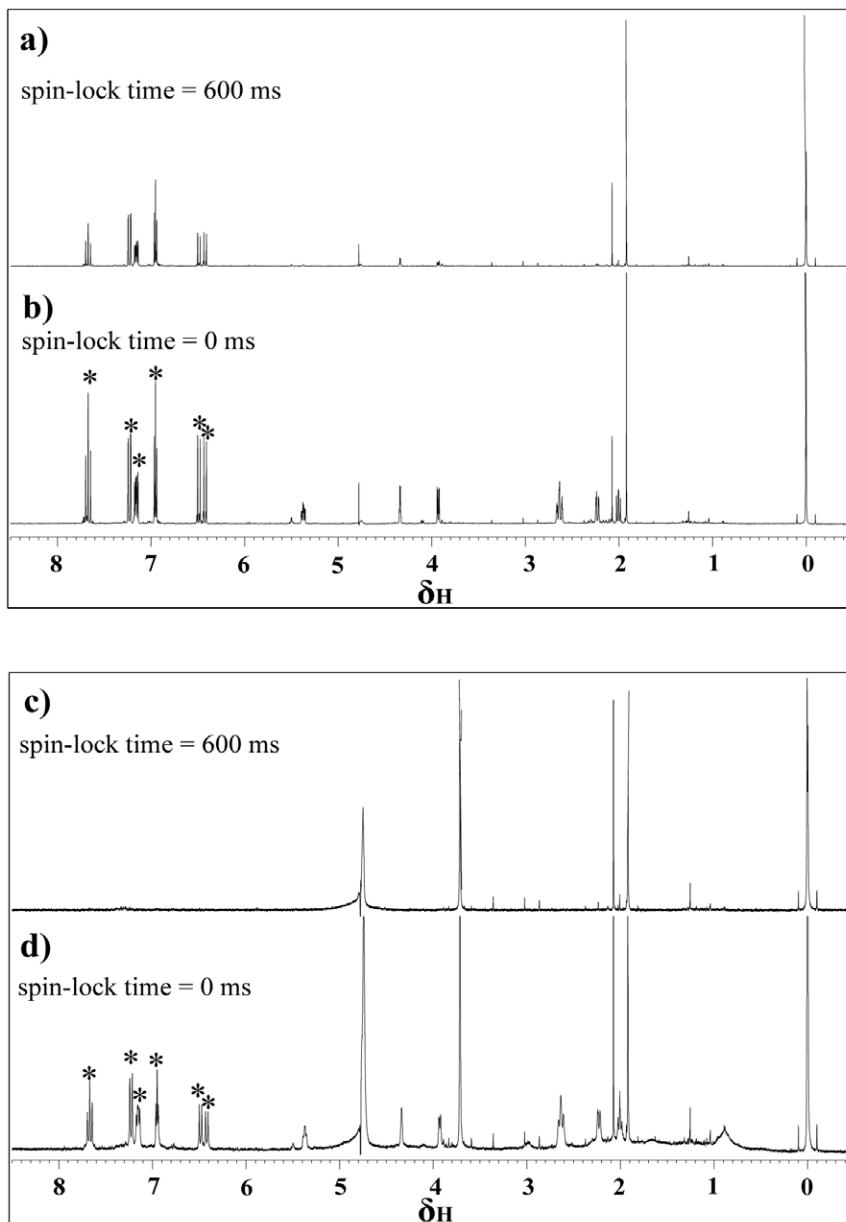
Figure 1. Binder screening by relaxation-edited NMR. Spectra of 1,5-dicaffeoylquinic acid (compound b) in the absence (plots **a**, **b**) and presence (plots **c**, **d**) of PA$_C$, with the CPMG spin-lock time labeled beside each spectrum. The concentration of the small molecule and PA$_C$ was 1.0×10^{-3} mol/L and 4.4×10^{-6} mol/L, respectively. The water peak located at δ 4.8 and 1 mM of TSP was added to the sample as a reference (δ 0). Signals of the small molecule in the absence of PA$_C$ attenuated slightly when 600 ms of CPMG spin-lock was applied (plot **a**). These signals were eliminated at the same spin-lock time in the presence of PA$_C$ (plot **c**). This difference should be ascribed to the increase in transverse relaxation rate (R_2) of the small molecule upon its binding to PA$_C$. The ligand peaks that attenuated when applying CPMG spin-lock in the presence of PA$_C$ were marked with "*" in plots **b** and **d**.
doi:10.1371/journal.pone.0035234.g001

water molecules were removed, polar hydrogen atoms were added, and non-polar hydrogen atoms were merged using the Hydrogen module in the AutoDock Tools (ADT). Then, Kollman united atom partial charges were assigned. The grid map of the docking simulation was established in a $61 \times 61 \times 61$ cube centered on the target active sites referred to in a previous report [10]. The targets are defined as site 1: center of K328, K539, R566 and K574; site 2: center of K539, R566, K574 and N696; site 3: center of E410, K461, E524 and K536; site 4: center of F411, M595, L666, W706, F710, V636 and L640; and site 5: center of 620 and 621. There is a spacing of 0.375 Å between the grid points. When the ligand was

docked to the PA$_C$ target, the Lamarckian genetic algorithm was used to optimize the conformation of the ligand in the binding pocket. The parameters were set to the following: the size of the population was 150; the number of energy evaluations was set to 1.0×10^8 as the run terminates; for clustering the conformations, the root mean square deviation tolerance was set to 2.0; fifty independent docking runs were carried out for every ligand; and other parameters were set to default. The binding affinities of the candidate compounds to the targets were summarized in Table S2, and the average pK_i of the five active sites was summarized in Table 2.
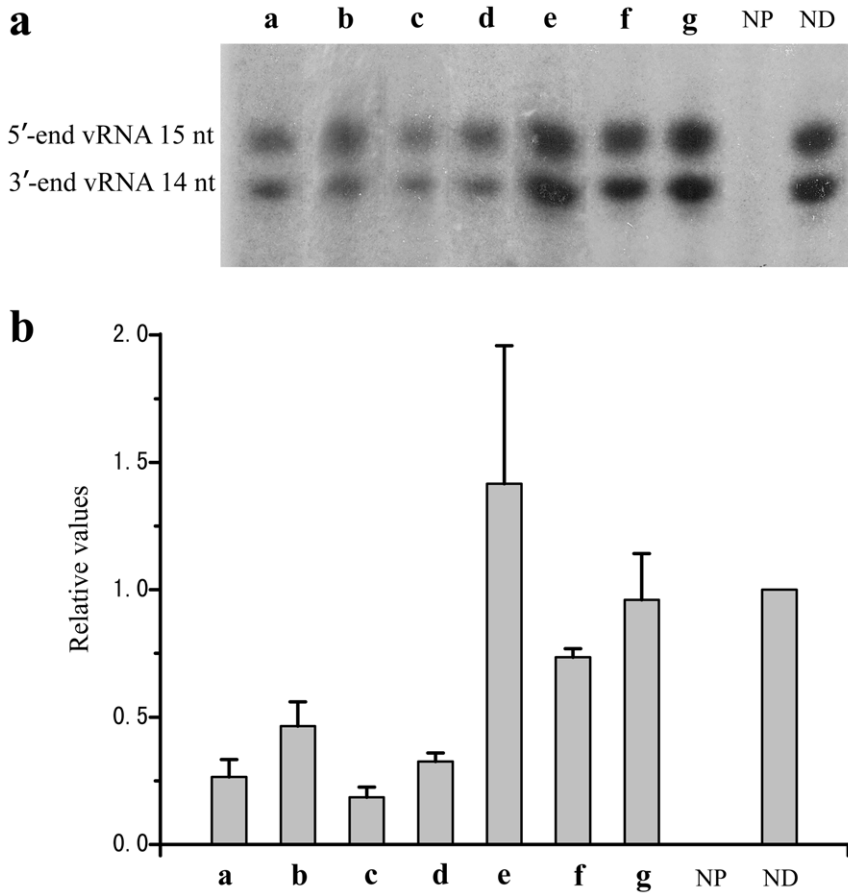
Figure 2. Results of ApG primer extension assay. (a) The effects of candidate compounds **a**, **b**, **c**, **d**, **e**, **f**, and **g** on polymerase activity in an ApG primer extension assay. The concentrations of the small molecules were 5 mM. NP stands for the negative reference with "no polymerase", and ND for the positive reference with "no drug." **(b)** The quantification of the results from **(a)** obtained by phosphorimaging analysis. The results are the average of two independent experiments and the derivations are shown.
doi:10.1371/journal.pone.0035234.g002

NMR experiments

NMR experiments were performed on a Bruker AVANCE 600 spectrometer equipped with a 5 mm BBI probe capable of delivering z-field gradients, using TOPSPIN software (Bruker, version 2.1) was used in experimental manipulating and data processing. All experiments were carried out at 298.2 K. The relaxation-edited NMR experiments utilized a [D/pre-saturation-90_x-(Δ-180_y-Δ)$_n$-acquire] pulse sequence, in which the CPMG sequence was used for the spin-lock. For all relaxation-edited experiments the following variables were used: pre-saturation water suppression was applied in pre-acquisition delay ($D = 3$ s), P_{90} was measured and set up for each sample, $\Delta = 1.5$ ms, and $2 \times n \times \Delta$ = total spin-lock time. The spectra were collected with 64 k of data points and 32 scans. Transverse relaxation times were measured by a pseudo-2D experiment using the CPMG sequence. Presaturation was applied in a pre-acquisition delay for water suppression, and 32 k and 16 data points were set for the F2 and F1 dimension, respectively. In each experiment, the following variables were used: $D = 3$ s (pre-acquisition delay); P_{90} was measured and set up for each sample; $\Delta = 1.5$ ms; the list of spin-lock loop (n) was set to 0, 10, 20, 30, 40, 50, 80, 100, 150, 200, 250, 300, 350, 400, 500, 600; and $2 \times n \times \Delta$ = total spin-lock time. The spectra were collected with 32 scans, and each T_2 was calculated using TOPSPIN (Bruker, version 2.1) software by simulating the peak attenuation curve in different spin-lock times.

The affinity analysis based on T_2 simulation

The method to evaluate K_d by T_2 simulation was previously reported [26]. When a ligand (L) and a protein (P) form a complex (LP), there is a dissociation equilibrium LP = L+P in the solution. The dissociation constant, K_d, of this equilibrium is a key factor to describe the binding strength of the ligand and protein. It can be evaluated by the transverse relaxation time (T_2) of the ligand in the presence of the protein. The expression describing the observed effective transverse relaxation rate R_{2obs} ($1/T_{2obs}$) as a function of molar ratio of protein to ligand (C_P/C_L) is:

$$2(R_{2obs} - R_{2F})/(R_{2B} - R_{2F}) =$$
$$1 + (K_d/C_P)(C_P/C_L) + n(C_P/C_L) -$$
$$\{[1 + (K_d/C_P)(C_P/C_L) + n(C_P/C_L)]^2 - 4n(C_P/C_L)\}^{1/2}$$

Since the total concentration of PA$_C$, C_P, and the ligand, C_L, in the experiments were known, it is possible to obtain the T_{2F} and T_{2B} from the plot of T_{2obs} versus C_P/C_L. Extrapolation of the curve to $C_P/C_L = 0$ should give T_{2F} and to infinite give T_{2B}. Then, by simulating the plot of R_{2obs} versus C_P/C_L using the above equation, K_d can be simultaneously obtained.

To evaluate the binding affinities between the candidate compounds and PA_C, a series of samples containing small molecules and PA_C with different concentration ratios (shown in Figure S9, S10, S11, S12, and S13) were prepared. These T_2 of the ligands were determined by the CPMG method using NMR. As we can see from Figure S9, S10, S11, S12, and S13, the observed T_2 (T_{2obs}) of the ligand decreases when the concentration ratio of protein to ligand (C_P/C_L) increases and the variation trends according to exponential decay. By simulating the plot of R_{2obs} ($R_{2obs} = 1/T_{2obs}$) versus C_P/C_L using equation (6), the K_d value can be obtained. The results of the simulation were summarized in Table 2.

The affinity analysis based on Surface Plasmon Resonance (SPR)

An affinity analysis of the interaction of candidate compounds a-g and PA_C was carried out using an SPR spectrometer (Biacore 3000, GE Healthcare Bio-Sciences, Sweden). PA_C at a concentration of 10 µg/mL in 10 mM NaAC, pH 5.5, was used to couple this protein to a CM5 sensor chip. To determine the affinity of small molecules to PA_C, increasing concentrations (labeled in Figure S14, S15, S16, S17, S18, S19, and S20) of the small molecules diluted in running buffer (130 mM PBS, pH 7.5) were injected over the sensor chip for 60 s (association phase), which was followed by dissociation for 180 s and recording of the spectra. All of the experiments were performed at 25°C, and the flow rate was 30 µL/min. The surface at the end of each experiment was regenerated using 20 mM NaOH at 30 µL/min for 10 s to remove any bound analyte. The data were analyzed using the BIAevaluation software (4.1 version) to calculate the affinity constant. The association and dissociation kinetics plots of the small molecules to PA_C were displayed in Figure S14, S15, S16, S17, S18, S19, and S20, and the results were summarized in Table 2.

Polymerase activity test

The ApG primer extension assay was previously described [24]. We performed 5 µL reactions with 2.5 µL 3P and 0.7 µM model vRNA promoter (an equimolar mixture of the 5′-end vRNA 5′-AGUAGAAACAAGGCC-3′ and 3′-end vRNA 5′-GGCCUG-CUUUUGCU-3′) in the presence of 5 mM $MgCl_2$, 5 mM drug, 5 mM dithiothreitol, 1 mM ATP, 0.5 mM UTP, 0.5 mM CTP, 0.1 µM[α-^{32}P]GTP (3,000 Ci/mmol), and 2 U/µL RNasin (Promega). Where indicated, 0.5 mM ApG (Sigma) was added to the reaction. The reaction system can be described as: 0.25 µL 0.1 M $MgCl_2$, 0.25 µL 0.1 M DTT, 0.5 µL 10 mM ApG, 0.25 µL RNasin, 0.25 µL 20×NTP, 0.25 µL 20×promoter, 0.25 µL [α-^{32}P]GTP, 2.5 µL polymerase, 0.5 µL depc H_2O or 0.5 µL small molecule. Reactions were incubated at 30°C for 1 h. The loading buffer, 5 µL 2×formamide/bromophenolblue/EDTA, and the mixture were heated at 95°C for 2 min. Analysis was performed by running the samples on an 18% PAGE with 1×Tris-borate-EDTA and 8 M urea followed by autoradiography.

Supporting Information

Figure S1 Binder screening by relaxation-edited NMR. Spectra of 3,4-dicaffeoylquinic acid (compound **a**) in the absence (plots **a**, **b**) and presence (plots **c**, **d**) of PA_C. The CPMG spin-lock time of each experiment was labeled beside the spectrum. The concentration of the small molecule and PA_C was 1.0×10^{-3} mol/L and 7.0×10^{-6} mol/L, respectively. The water peak located at δ 4.8 and 1 mM of TSP was added to the sample as a reference (δ

0). The ligand peaks that attenuated when applying CPMG spin-lock in the presence of PA_C were marked with "*" in plot **d**. (TIF)

Figure S2 Binder screening by relaxation-edited NMR. Spectra of 4,5-dicaffeoylquinic acid (compound **c**) in the absence (plots **a**, **b**) and presence (plots **c**, **d**) of PA_C. The CPMG spin-lock time of each experiment was labeled beside the spectrum. The concentration of the small molecule and PA_C was 1.0×10^{-3} mol/L and 7.0×10^{-6} mol/L, respectively. The water peak located at δ 4.8 and 1 mM of TSP was added to the sample as a reference (δ 0). The ligand peaks that attenuated when applying CPMG spin-lock in the presence of PA_C were marked with "*" in plot **d**. (TIF)

Figure S3 Binder screening by relaxation-edited NMR. Spectra of 3,5-dicaffeoylquinic acid (compound **d**) in the absence (plots **a**, **d**) and presence (plots **c**, **d**) of PA_C. The CPMG spin-lock time of each experiment was labeled beside the spectrum. The concentration of the small molecule and PA_C was 1.0×10^{-3} mol/L and 7.0×10^{-6} mol/L, respectively. The water peak located at δ 4.8 and 1 mM of TSP was added to the sample as a reference (δ 0). The ligand peaks that attenuated when applying CPMG spin-lock in the presence of PA_C were marked with "*" in plot **d**. (TIF)

Figure S4 Binder screening by relaxation-edited NMR. Spectra of 1,3-dicaffeoylquinic acid (compound **e**) in the absence (plots **a**, **b**) and presence (plots **c**, **d**) of PA_C. The CPMG spin-lock time of each experiment was labeled beside the spectrum. The concentration of the small molecule and PA_C was 1.0×10^{-3} mol/L and 5.5×10^{-6} mol/L, respectively. The water peak located at δ 4.8 and 1 mM of TSP was added to the sample as a reference (δ 0). The ligand peaks that attenuated when applying CPMG spin-lock in the presence of PA_C were marked with "*" in plots **d**. (TIF)

Figure S5 Binder screening by relaxation-edited NMR. Spectra of 5-caffeoylquinic acid (compound **f**) in the absence (plots **a**, **b**) and presence (plots **c**, **d**) of PA_C. The CPMG spin-lock time of each experiment was labeled beside the spectrum. The concentration of the small molecule and PA_C was 1.0×10^{-3} mol/L and 8.7×10^{-6} mol/L, respectively. The water peak located at δ 4.8 and 1 mM of TSP was added to the sample as a reference (δ 0). The ligand peaks that attenuated when applying CPMG spin-lock in the presence of PA_C were marked with "*" in plot **d**. (TIF)

Figure S6 Binder screening by relaxation-edited NMR. Spectra of 4-caffeoylquinic acid (compound **g**) in the absence (plots **a**, **b**) and presence (plots **c**, **d**) of PA_C. The CPMG spin-lock time of each experiment was labeled beside the spectrum. The concentration of the small molecule and PA_C was 1.0×10^{-3} mol/L and 8.7×10^{-6} mol/L, respectively. The water peak located at δ 4.8 and 1 mM of TSP was added to the sample as a reference (δ 0). The ligand peaks that attenuated when applying CPMG spin-lock in the presence of PA_C were marked with "*" in plot **d**. (TIF)

Figure S7 Binder screening by relaxation-edited NMR. Spectra of quinic acid (compound **h**) in the absence (plots **a**, **b**) and presence (plots **c**, **d**) of PA_C. The CPMG spin-lock time of each experiment was labeled beside the spectrum. The concentration of the small molecule and PA_C was 1.0×10^{-3} mol/L and

8.7×10^{-6} mol/L, respectively. The water peak located at δ 4.8 and 1 mM of TSP was added to the sample as a reference (δ 0). (TIF)

Figure S8 Binder screening by relaxation-edited NMR. Spectra of caffeic acid (compound **i**) in the absence (plots ***a***, ***b***) and presence (plots ***c***, ***d***) of PA$_C$. The CPMG spin-lock time of each experiment was labeled beside the spectrum. The concentration of the small molecule and PA$_C$ was 1.0×10^{-3} mol/L and 8.7×10^{-6} mol/L, respectively. The water peak located at δ 4.8 and 1 mM of TSP was added to the sample as a reference (δ 0). (TIF)

Figure S9 The most possible binding site of 3,4-dicaffeoylquinic acid on PA$_C$ supposed by visual docking. (TIF)

Figure S10 The most possible binding site of 1,5-dicaffeoylquinic acid on PA$_C$ supposed by visual docking. (TIF)

Figure S11 The most possible binding site of 4,5-dicaffeoylquinic acid on PA$_C$ supposed by visual docking. (TIF)

Figure S12 The most possible binding site of 3,5-dicaffeoylquinic acid on PA$_C$ supposed by visual docking. (TIF)

Figure S13 The most possible binding site of 1,3-dicaffeoylquinic acid on PA$_C$ supposed by visual docking. (TIF)

Figure S14 The most possible binding site of 5-caffeoylquinic acid on PA$_C$ supposed by visual docking. (TIF)

Figure S15 The most possible binding site of 4-caffeoylquinic acid on PA$_C$ supposed by visual docking. (TIF)

Figure S16 The most possible binding site of quinic acid on PA$_C$ supposed by visual docking. (TIF)

Figure S17 The most possible binding site of caffeic acid on PA$_C$ supposed by visual docking. (TIF)

Figure S18 Binding affinity between 1,5-dicaffeoylquinic acid and PA$_C$ evaluated by transverse relaxation simulation. a) The plot of T_{2obs} versus C_P/C_L; **b**) The plot of R_{2obs} versus C_P/C_L. (TIF)

Figure S19 Binding affinity between 1,3-dicaffeoylquinic acid and PA$_C$ evaluated by transverse relaxation simulation. a) The plot of T_{2obs} versus C_P/C_L; **b**) The plot of R_{2obs} versus C_P/C_L. (TIF)

Figure S20 Binding affinity between 3,5-dicaffeoylquinic acid and PA$_C$ evaluated by transverse relaxation

simulation. a) The plot of T_{2obs} versus C_P/C_L; **b**) The plot of R_{2obs} versus C_P/C_L. (TIF)

Figure S21 Binding affinity between 3,4-dicaffeoylquinic acid and PA$_C$ evaluated by transverse relaxation simulation. a) The plot of T_{2obs} versus C_P/C_L; **b**) The plot of R_{2obs} versus C_P/C_L. (TIF)

Figure S22 Binding affinity between 4,5-dicaffeoylquinic acid and PA$_C$ evaluated by transverse relaxation simulation. a) The plot of T_{2obs} versus C_P/C_L; **b**) The plot of R_{2obs} versus C_P/C_L. (TIF)

Figure S23 Association and dissociation kinetics plot of 3,4-dicaffeoylquinic acid to PAC as determined by SPR. (TIF)

Figure S24 Association and dissociation kinetics plot of 1,5-dicaffeoylquinic acid to PAC as determined by SPR. (TIF)

Figure S25 Association and dissociation kinetics plot of 4,5-dicaffeoylquinic acid to PAC as determined by SPR. (TIF)

Figure S26 Association and dissociation kinetics plot of 3,5-dicaffeoylquinic acid to PAC as determined by SPR. (TIF)

Figure S27 Association and dissociation kinetics plot of 1,3-dicaffeoylquinic acid to PAC as determined by SPR. (TIF)

Figure S28 Association and dissociation kinetics plot of 5-caffeoylquinic acid to PA$_C$ as determined by SPR. (TIF)

Figure S29 Association and dissociation kinetics plot of 4-caffeoylquinic acid to PA$_C$ as determined by SPR. (TIF)

Figure S30 Binder screening by relaxation-edited NMR. Spectra of 3,4-dicaffeoylquinic acid (compound **a**) in the absence (plots ***a***, ***b***) and presence (plots ***c***, ***d***) of HSA. The CPMG spin-lock time of each experiment was labeled beside the spectra. The concentrations of small molecule and HSA were 1.0×10^{-3} mol/L and 7.0×10^{-6} mol/L, respectively. The water peak located at δ 4.8. The peaks of small molecule were not eliminated at a long spin-lock time, indicated that compound **a** did not specifically interact with HSA. (TIF)

Table S1 Structure of candidate compounds. (DOC)

Table S2 Binding affinities of chlorogenic acid to different active sites of PA$_C$ evaluated by virtual docking. (DOC)

Author Contributions

References

1. Subbarao K, Klimov A, Katz J, Regnery H, Lim W, et al. (1998) Characterization of an avian influenza A (H5N1) virus isolated from a child with a fatal respiratory illness. Science 279: 393–396.
2. De Clercq E (2006) Antiviral agents active against influenza A viruses. Nat Rev Drug Discov 5: 1015–1025.
3. De Clercq E, Neyts J (2007) Avian influenza A (H5N1) infection: targets and strategies for chemotherapeutic intervention. Trends Pharmacol Sci 28: 280–285.
4. Kiso M, Mitamura K, Sakai-Tagawa Y, Shiraishi K, Kawakami C, et al. (2004) Resistant influenza A viruses in children treated with oseltamivir: descriptive study. Lancet 364: 759–765.
5. Le QM, Kiso M, Someya K, Sakai YT, Nguyen TH, et al. (2005) Avian flu: isolation of drug-resistant H5N1 virus. Nature 437: 1108.
6. De Jong MD, Thanh TT, Khanh TH, Hien VM, Smith GJD, et al. (2005) Brief report: Oseltamivir resistance during treatment of influenza A (H5N1) infection. New Engl J Med 353: 2667–2672.
7. Obayashi E, Yoshida H, Kawai F, Shibayama N, Kawaguchi A, et al. (2008) The structure basis for an essential subunit interaction in influenza virus RNA polymerase. Nature 454: 1127–1132.
8. Dias A, Bouvier D, Crépin T, McCarthy AA, Hart DJ, et al. (2009) The cap-snatching endonuclease of influenza virus polymerase resides in the PA subunit. Nature 458: 914–918.
9. He XJ, Zhou J, Bartlam M, Zhang RG, Ma JY, et al. (2008) Crystal structure of the polymerase PAC–PB1N complex from an avian influenza H5N1 virus. Nature 454: 1123–1127.
10. Yuan PW, Bartlam M, Lou ZY, Chen SD, Zhou J, et al. (2009) Crystal structure of an avian influenza polymerase PAN reveals an endonuclease active site. Nature 458: 909–914.
11. Nakazawa M, Kadowaki SE, Watanabe I, Kadowaki Y, Takei M, et al. (2008) PA subunit of RNA polymerase as a promising target for anti-influenza virus agents. Antivir Res 78: 194–201.
12. Fodor E, Crow M, Mingay LJ, Deng T, Sharps J, et al. (2002) A single amino acid mutation in the PA subunit of the influenza virus RNA polymerase inhibits endonucleolytic cleavage of capped RNAs. J Virol 76: 8989–9001.
13. Hara K, Schmidt FI, Crow M, Brownlee GG (2006) Amino acid residues in the N-terminal region of the PA subunit of influenza A virus RNA polymerase play a critical role in protein stability, endonuclease activity, cap binding, and virion RNA promoter binding. J Virol 80: 7789–7798.
14. Hara K, Shiota M, Kido H, Ohtsu Y, Kashiwagi T, et al. (2001) Influenza virus RNA polymerase PA subunit is a novel serine protease with Ser624 at the active site. Genes Cells 6: 87–97.
15. Rodriguez A, Perez-Gonzalez A, Nieto A (2007) Influenza Virus Infection Causes Specific Degradation of the Largest Subunit of Cellular RNA Polymerase II. J Virol 81: 5315–5324.
16. Regan JF, Liang Y, Parslow TG (2006) Defective assembly of Influenza A virus due to a mutation in the polymerase subunit PA. J Virol 80: 252–261.
17. Li L, Chang SH, Xiang JF, Li Q, Liang HH, et al. (2011) Screening Anti-influenza Agents that Target at Avian Influenza Polymerase Protein PAC from Plant Extracts Based on NMR Methods. Chem Lett 40:801–803.
18. Iwai Y, Murakami K, Gomi Y, Hashimoto T, Asakawa Y, et al. (2011) Anti-Influenza Activity of Marchantins, Macrocyclic Bisbibenzyls Contained in Liverworts. PLoS ONE 6(5): e19825.
19. Su CY, Cheng RTJ, Lin MI, Wang SY, Huang WI, et al. (2010) High-throughput Identification of Compounds Targeting Influenza RNA-Dependent RNA Polymerase Activity. PNAS 107: 19151–19156.
20. Ko HC, Wei BL, Chiou WF (2006) The effect of medicinal plants used in Chinese folk medicine on RANTES secretion by virus-infected human epithelial cells. J Ethnopharmacol 107: 205–210.
21. Ge F, Ke CQ, Tang W, Yang XZ, Tang CP, et al. (2007) Isolation of chlorogenic acids and their derivatives from stemona japonica by preparative HPLC and evaluation of their anti-AIV (H5N1) activity in vitro. Phytochem Anal 18: 213–218.
22. Lepre CA, Moore JM, Peng JW (2004) Theory and applications of NMR-based screening in pharmaceutical research. Chem Rev 104: 3641–3675.
23. Meyer B, Peters T (2003) NMR spectroscopy techniques for screening and identifying ligand binding to protein receptors. Angew Chem Int Ed 42: 864–890.
24. Deng T, Vreede FT, Brownlee GG (2006) Different de novo initiation strategies are used by influenza virus RNA polymerase on its cRNA and viral RNA promoters during viral RNA replication. J Virol 80: 2337–2348.
25. Zhang SJ, Wang JL, Wang Q, Toyoda T (2010) Internal initiation of influenza virus replication of viral RNA and complementary RNA in vitro. J Bio Chem 285: 41194–41201.
26. Luo RS, Liu ML, Mao XA (1999) NMR diffusion and relaxation study of drug-protein interaction. Spectrochim Acta A 55: 1897–1901.